Original Research Article

^{18}FDG positron emission tomography mining for metabolic imaging biomarkers of radiation-induced xerostomia in patients with oropharyngeal cancer

Hesham Elhalawani [a,b,*,1], Carlos E. Cardenas [c,1], Stefania Volpe [a,d], Souptik Barua [e,f], Sonja Stieb [a], Calvin B. Rock [a,k], Timothy Lin [a], Pei Yang [a,g], Haijun Wu [a], Jhankruti Zaveri [h], Baher Elgohari [a,i], Lamiaa E. Abdallah [j], Amit Jethanandani [a], Abdallah S.R. Mohamed [a], Laurence E. Court [c], Katherine A. Hutcheson [h], G. Brandon Gunn [a], David I. Rosenthal [a], Steven J. Frank [a], Adam S. Garden [a], Arvind Rao [e,f,l,m,n], Clifton D. Fuller [a,*]

[a] *Department of Radiation Oncology, University of Texas MD Anderson Cancer Center, Houston, TX, United States*
[b] *Department of Radiation Oncology, Brigham and Women's Hospital and Dana-Farber Cancer Institute, Boston, MA, United States*
[c] *Department of Radiation Physics, University of Texas MD Anderson Cancer Center, Houston, TX, United States*
[d] *Department of Oncology and Hemato-oncology, University of Milan, Milan, Italy*
[e] *Department of Electrical and Computer Engineering, Rice University, Houston, TX, United States*
[f] *Department of Computational Medicine and Bioinformatics, University of Michigan, Ann Arbor, MI, United States*
[g] *Key Laboratory of Translational Radiation Oncology, Hunan Cancer Hospital, Xiangya Medical School, Central South University, Changsha, China*
[h] *Department of Head and Neck Surgery, Section of Speech Pathology and Audiology, The University of Texas MD Anderson Cancer Center, Houston, TX, United States*
[i] *Department of Clinical Oncology & Nuclear Oncology, Mansoura University, Mansoura, Egypt*
[j] *Department of Clinical Oncology & Nuclear Oncology, Ain Shams University, Cairo, Egypt*
[k] *Department of Radiation Oncology, University of Utah Huntsman Cancer Institute, Salt Lake City, UT, United States*
[l] *Department of Radiation Oncology, University of Michigan Medical School, Ann Arbor, MI, United States*
[m] *Department of Biostatistics, School of Public Health, University of Michigan, Ann Arbor, MI, United States*
[n] *Department of Biomedical Engineering, University of Michigan, Ann Arbor, MI, United States*

ARTICLE INFO

ABSTRACT

Purpose: Head and neck cancers radiotherapy (RT) is associated with inevitable injury to parotid glands and subsequent xerostomia. We investigated the utility of SUV derived from ^{18}FDG-PET to develop metabolic imaging biomarkers (MIBs) of RT-related parotid injury.

Methods: Data for oropharyngeal cancer (OPC) patients treated with RT at our institution between 2005 and 2015 with available planning computed tomography (CT), dose grid, pre- & first post-RT ^{18}FDG-PET-CT scans, and physician-reported xerostomia assessment at 3–6 months post-RT (Xero 3–6 ms) per CTCAE, was retrieved, following an IRB approval. A CT-CT deformable image co-registration followed by voxel-by-voxel resampling of pre & post-RT ^{18}FDG activity and dose grid were performed. Ipsilateral (Ipsi) and contralateral (contra) parotid glands were sub-segmented based on the received dose in 5 Gy increments, i.e. 0–5 Gy, 5–10 Gy sub-volumes, etc. Median and dose-weighted SUV were extracted from whole parotid volumes and sub-volumes on pre- & post-RT PET scans, using in-house code that runs on MATLAB. Wilcoxon signed-rank and Kruskal-Wallis tests were used to test differences pre- and post-RT.

Results: 432 parotid glands, belonging to 108 OPC patients treated with RT, were sub-segmented & analyzed. Xero 3–6 ms was reported as: non-severe (78.7%) and severe (21.3%). SUV- median values were significantly reduced post-RT, irrespective of laterality (p = 0.02). A similar pattern was observed in parotid sub-volumes, especially ipsi parotid gland sub-volumes receiving doses 10–50 Gy (p < 0.05). Kruskal-Wallis test showed a significantly higher mean RT dose in the contra parotid in the patients with more severe Xero 3-6mo (p = 0.03).

Multiple logistic regression showed a combined clinical-dosimetric-metabolic imaging model could predict the severity of Xero 3-6mo; AUC = 0.78 (95%CI: 0.66–0.85; p < 0.0001).

Conclusion: We sought to quantify pre- and post-RT ^{18}FDG-PET metrics of parotid glands in patients with OPC. Temporal dynamics of PET-derived metrics can potentially serve as MIBs of RT-related xerostomia in concert with clinical and dosimetric variables.

Introduction

Head and neck cancer (HNC) radiotherapy (RT) is associated with inevitable injury to the parotid glands due to the radiation beam pathways, with subsequent xerostomia. Xerostomia is also the most often reported radiation-induced side effect in these patients, with 50% exhibiting acute Grade (G) 2/3 and 32% late G2/3 xerostomia [1]. This can further contribute to other radiation-induced symptoms like dysphagia, speech problems, and taste alteration, in addition to secondary problems like dental caries [2–4]. Although there is a potential for recovery even years after RT, xerostomia remains a major detrimental factor to patients' quality of life after HNC RT [5]. With the broad use of positron emission tomography (PET) as an imaging modality to assess treatment response in HNC [6,7], the question arises if PET can also be used to quantify changes in organs at risk after radiotherapy and to assess the degree of xerostomia [8–10].

In this study we therefore investigated the utility of standardized uptake values (SUV) derived from routinely performed 18-fluorodeoxy-gluocose PET (^{18}FDG-PET) scans for staging and response evaluation to develop metabolic imaging biomarkers (MIBs) of RT-related parotid injury. The specific aims of our study can be summarized as follows:

1. Outline an analytical workflow for radiotherapy-associated normal tissues toxicities assessment studies incorporating PET imaging
2. Investigate the dose–response relationship between RT dose and longitudinal alterations of quantitative PET SUV metrics (Δ changes) in the parotid gland
3. Assess the utility of Δ SUV changes to model the severity of subacute RT-induced parotid injury and subsequent xerostomia at 3–6 months.

Methods

Study population

Following an approval from an institutional review board (IRB) at the University of Texas M.D. Anderson Cancer Center, data for biopsy proven oropharyngeal cancer (OPC) patients treated between 2005 and 2015 who underwent radiation therapy as a single or multimodality definitive therapy were considered for the current investigation (n = 150). This investigation and relevant methodology were performed in compliance with the Health Insurance Portability and Accountability Act (HIPAA) as a retrospective study where the need for informed consent was waived [11]. Electronic medical records were scanned for various demographic, disease, and treatment characteristics in the absence of any prior head and neck re-irradiation. (Table 1) The aspects of our institutional multidisciplinary approach for managing oropharyngeal cancer patients –including RT planning- were previously reported in detail [12,13]. Eligibility criteria required individuals to have received pre-treatment and post-RT ^{18}FDG-PET-CT scans, and have retrievable planning CT and dose grid, as well as Xerostomia assessment at 3–6-months following RT course start (Xero 3-6mo). Common Terminology Criteria for Adverse Events (CTCAE v5.0) were applied to grade Xerostomia using a Likert scale that ranged between 0 (no) and 3 (severe) [14].

Treatment and planning

The overall treatment strategy was decided following multidisciplinary team case discussion. Surgically treated patients were ineligible for this analysis. All patients were treated using intensity-modulated radiotherapy (IMRT) using previously described protocols [12,13]. All patients initially underwent CT-based simulation, immobilized in a supine position with 5-point head, neck, and shoulders thermoplastic masks, bite block with or without an oral stent. Non contrast-enhanced CT using 3 mm slice thickness was carried out, ranging from the vertex to the manubrial sternal joint for planning. Target volumes were

Table 1
Patients, disease and treatment characteristics.

Characteristics	N (%)
Sex	
Male	96 (88.89%)
Female	12 (11.11%)
Age at diagnosis, years: median (interquartile range 'IQR')*	59.3 (53.4–64)
Tumor laterality	
Right	50 (46.3%)
Left	58 (53.7%)
Oropharynx subsites	
Base of tongue	57 (52.8%)
Tonsil	41 (38%)
Others	10 (9.2%)
p16 status	
Positive	99 (91.7%)
Negative	6 (5.6%)
NA	3 (2.8%)
T category	
T0	3 (2.8%)
T1	32 (29.6%)
T2	47 (43.5%)
T3	16 (14.8%)
T4	9 (8.4%)
Tx	1 (0.9)
N category (ICON-S)	
N0	1 (0.9%)
N1	72 (66.7%)
N2	33 (30.6%)
N3	2 (1.8%)
Therapeutic combination	
Radiation alone	12 (11.1%)
Induction chemotherapy (IC) followed by concurrent chemoradiation (CC)	28 (25.9%)
IC followed by radiation alone	17 (15.7%)
CC	51 (47.3%)
Radiation dose (median; IQR) [Gy]*	70 (66–70)
Radiation fractions (median; IQR)	33 (30–33)
Baseline xerostomia	
Yes	23 (21.3%)
No	82 (75.9%)
Not reported	3 (2.8%)
Xerostomia at 3–6 months (CTCAE v5.0)*	
0	1 (0.9%)
1	45 (41.7%)
2	36 (33.3%)
3	23 (21.3%)
Not reported	3 (2.8%)
Mean parotid dose (Gy; standard deviation)	
Ipsilateral	35.4 (13.1)
Contralateral	19.7 (10.4)

*IQR: inter-quartile range; Gy: Gray; CTCAE v5.0: 5th version of common terminology criteria for adverse events.

delineated and reviewed by MD Anderson's Radiation Oncology Head-and-Neck Planning and Development Clinic. In brief, the process entails comprehensive review of a patient's history, pathology, diagnostic imaging, and discussion of the planned treatment. All patients undergo physical examination (PE) including video-camera nasopharyngolaryngoscopy and bimanual palpation performed by a team of head-and-neck radiation oncology sub-specialists. The proposed segmentations were reviewed slice-by-slice for gross tumor volume (GTV), clinical target volume (CTV) and OAR segmentation, as well as dose-volume specifications. By this manner, intra- and inter-observer variability in segmentation are minimized because of the utilization of multi-observer agreement contours rather than single-observer contours. General treatment strategies included defining 3 clinical target volumes (CTVs). CTV1 included gross lymph node disease with a margin or, in post-operative situations, the preoperative tumor bed with margin. A virtual gross target volume (GTV) was created for patients who received chemotherapy before radiation, and margins similar to those used in patients who had true GTVs were added to create CTV1 in this setting. CTV2 was a neck volume at high risk of harboring microscopic disease but without clinical, radiographic, or pathologic evidence of lymph node disease; and CTV3 was the lymph node volume and mucosa deemed at low risk of harboring subclinical disease. All CTVs were treated simultaneously, with fractional doses ranging from 1.7 to 2.2 Gray (Gy), depending on the number of fractions and the total dose prescribed to each respective CTV. PTV include CTV + 3 mm margin.

IMRT was applied to treat the primary tumor and the upper neck nodal disease matched to an anteroposterior low anterior neck field with a larynx midline block (IMRT split-field technique). Whole-field IMRT was used for junctional tumors to avoid under-dosing. Small volume primary tumors were usually prescribed up to 66 Gy, while more advanced tumors were prescribed up to 70–72 Gy, and elective regions received 54–63 Gy, delivered over 6–7 weeks (5 or 6 fractions a week). Radiation was delivered using 6-MV photons linear accelerators. No systematic re-planning was performed for IMRT patients.

The objective parameter used in IMRT optimization for the parotid gland was at least one parotid gland $D_{mean} < 26$ Gy or $D_{50} < 30$ Gy. All patients underwent cone beam CT scans with linear accelerators once a week to correct setup errors before radiotherapy. Individualized decisions of additional systemic therapy were based on the disease burden, associated medical comorbidities and performance status. Concurrent systemic agents were assigned for patients with advanced primary tumor and/or bulky lymph node metastasis, while chemotherapy in the neoadjuvant setting was prescribed to patients with high risk of distant recurrence (e.g. advanced N-stage).

PET-CT acquisition protocol and eligibility criteria

Each patient underwent two [18]FDG-PET/CT scans, the first within 4 weeks prior to starting therapy and the second within 3–6 months following RT course initiation (median interval of around 135 days). FDG-PET/CT images were uniformly acquired and analyzed with a single scanner (Discovery ST-8; GE Medical Systems, Milwaukee, WI), as previously described [15].

Image registration and parotid glands segmentation

After CT-CT deformable image co-registration using commercial software (Velocity AI). Then resampling of pre & post-RT [18]FDG-PET scans and dose grid was done so that these scans matched the pixel and slice spacing of the treatment planning CT (Fig. 1). Parotid glands were categorized as ipsilateral 'ipsi' if ipsilateral to a well-lateralized primary tumor and/or unilateral neck irradiation filed. In case of more central
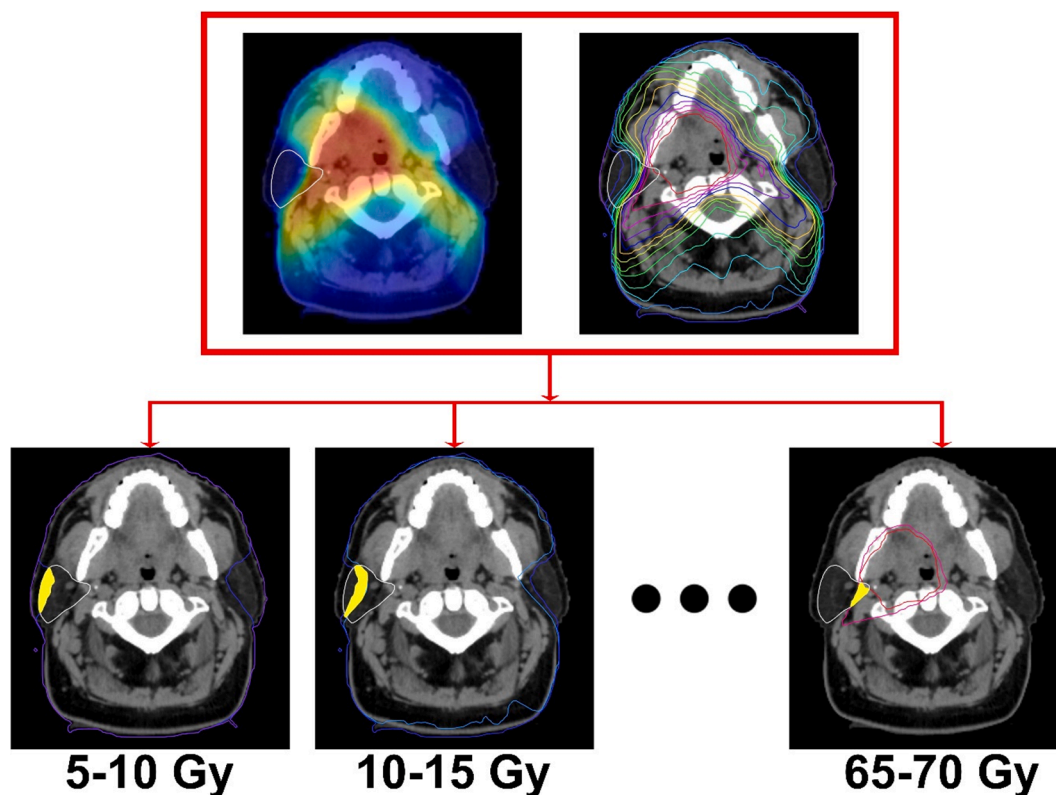

Fig. 1. Parotid dose sub-volume generation. Using the treatment plans' dose map and isodose lines, we define the sub-volumes by identifying the union between parotid structure (white) and the voxels within the desired isodose lines. For example, for the parotid sub-volume (yellow) receiving doses between 5 and 10 Gy, between 10 and 15 Gy, and between 65 and 70 Gy are shown with their respective isodose lines for each panel. (For interpretation of the references to colour in this figure legend, the reader is referred to the web version of this article.)

primary tumors (e.g. base of tongue) and/or bilateral neck irradiation, the parotid gland with higher delivered radiation dose, was labeled 'ipsi'. Otherwise, the gland will be categorized as contralateral 'contra'. Ipsilateral and contralateral parotid glands were sub-segmented into smaller sub-volumes based on the dose they received using 5 Gy increments, i.e. 0–5 Gy, 5–10 Gy sub-volumes, *etc*. These sub-volumes were automatically defined using in-house software (MATLAB, MathWorks, Natick, MA) which extracted each glands' contoured masks and overlaid these structures with each patient's isodose lines to extract the desired sub-volumes (Fig. 2). Using the treatment plans' dose map and isodose lines, we define the sub-volumes by identifying the union between parotid structure and the voxels within the desired isodose lines. These dose sub-volumes were defined on the pre & post-RT CT scans (from PET/CT) after deformably registering these scans to the treatment planning CT scan. We visually inspected parotid glands volumes and subvolumes and appropriateness of overlaid dose grids after each step, to account for patient positioning variability between simulation and diagnostic imaging, and to consider the limitations on PET spatial resolution. We excluded patients with detectable parotid displacement, e.g. in cases of significant in- or post-treatment weight loss or tumor shrinkage where re-planning was merited.

^{18}FDG-PET metabolic features extraction

Absolute and dose-weighted median SUV were extracted from these whole parotid glands and sub-volumes on pre- & post-RT PET scans, using in-house software. Dose-weighted SUV is defined by the voxel-wise multiplication of the registered PET scan's SUV map and radiotherapy planned dose map (Eq. (1)),

$$DwSUV_i = Dose_i \times SUV_i \tag{1}$$

where *i* represents each voxel in the image space. An illustration of the dose-weighted SUV is shown in Fig. 2.

Statistical analysis

Differences between median values of SUV-median pre-and post-RT for the whole glands volumes and sub-volumes were tested using Wilcoxon signed-rank test. We then applied Spearman's Rho rank correlation analysis to compute the correlation coefficient and corresponding p-values to find if percent changes in values on a whole or sub-volume level are significantly correlated with mean accumulated dose at the relevant volume of interest. Single then multiple logistic regressions were used to model the correlation between clinical, dosimetric, and SUV variables (e.g. age, induction chemotherapy, and baseline

xerostomia) and Xero 3-6mo. A p value of < 0.05 was considered significant. 95% CI of ROC AUC was obtained by 10,000 bootstrapping.

Results

Patients

432 parotid glands, belonging to 108 patients with OPC treated with RT, were delineated, sub-segmented & analyzed. Assessments of xerostomia at 3–6 months following initiation of radiation treatment were available for 105 patients and were reported as: non-severe, i.e. CTCAE grades 0, 1, and 2 (78.7%) and severe, i.e. CTCAE grade 3 (21.3%). Various demographics, disease, and treatment characteristics are reported in Table 1.

Parotids dosimetry and SUV metrics analytics

Ipsi and contra parotid glands received mean doses 'Gy' (Std) of 35.4 (13.2) & 20 (10.4), respectively. SUV-median tends to decrease significantly after RT (p = 0.02) for ipsi and contra parotid glands, where 62% and 57% of the parotid glands, respectively demonstrated a decline in SUV-median post-therapy, respectively (Supplementary Table S1).

We also observed a similar pattern of variation in SUV metrics across time on a parotid sub-volume level. Post-RT SUV-median values of parotid sub-volumes which received doses '5–50 Gy' decreased significantly as compared to their pre-RT counterparts, on combining both sides. This mainly applied to ipsi parotid gland sub-volumes receiving doses '10–50 Gy' (p < 0.05) (Supplementary Table S2).

A Spearman rank correlation test showed that overall; percent change in SUV-median was not correlated to mean accumulated dose at parotid glands. Similarly, negligible correlation between the sub-volumes median SUV changes and mean or discrete dose levels was found. This suggests that higher doses do not imply a higher magnitude of percent changes in SUV metrics, and vice-versa.

Modeling of xerostomia using clinical, dosimetric, and metabolic imaging features

Three patients with no recorded xerostomia assessment at 3–6 months were excluded (n = 3). For the remaining 105 patients, Xero 3-6mo was graded per CTCAE v5.0 as: 0 (1%), 1 (42.9%), 2 (34.3%), and 3 (21.9%). For the purpose of our analysis, we recategorized Xero 3-6mo into: non-severe (CTCAE G < 3; 78.1%) and severe (CTCAE G3; 21.9%). A Kruskal-Wallis test showed a significantly higher mean planned RT dose in the contra parotid in the subgroup who suffered from more severe Xero 3-6mo (p = 0.03). Patients with more severe Xero 3-6mo were

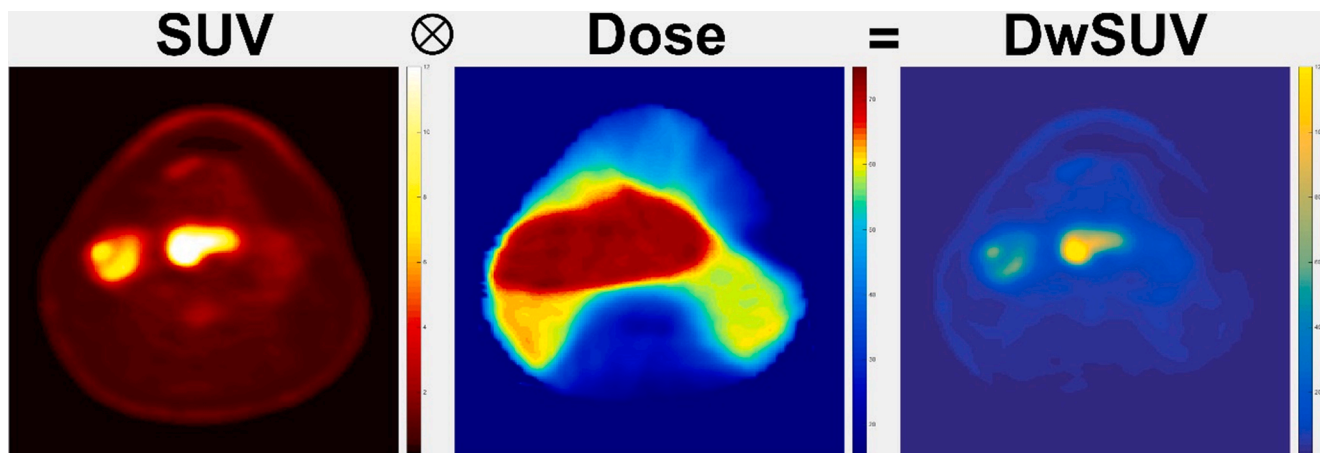

Fig. 2. Illustration of dose-weighted SUV computation. For each voxel in the co-registered image space, the SUV map and dose map matrices are multiplied using the Hadamard product [46] resulting in the dose-weighted SUV (DwSUV) maps.

also shown to have higher mean planned ipsi parotid glands doses (p = 0.1), and lower post-RT parotid SUV-median both for ipsi (p = 0.04) and contra (p = 0.02) parotid glands. Nevertheless, neither absolute nor dose-weighted percent changes in SUV-median correlated to Xero 3-6mo severity. Older age was also associated with more severe Xero 3-6mo (p = 0.01). Distribution of other clinical variables like therapeutic combination, AJCC stage (8th ed.), or presence of pre-treatment xerostomia didn't significantly differ between patients with severe and non-severe Xero 3-6mo. (Fig. 3)

A simple logistic regression (SLR) of individual clinical and dosimetric co-variates -known to affect salivary function and subsequent response to RT injury- in addition to extracted SUV metrics was performed. Older age (p = 0.04), higher mean planned RT dose at contra parotid glands (p = 0.001), and post-RT ipsi (p = 0.03) and contra (p = 0.1) parotid SUV median were significantly correlated to Xero 3-6mo. Though non-significant, higher mean ipsi parotid gland dose (p = 0.07) and more advanced cancer stage (p = 0.1) predicted more severe Xero 3-6mo.

We then performed a multiple logistic regression analysis including only statistically significant variables on SLR. Overall, this combined clinical-dosimetric-metabolic imaging model could adequately predict the severity of Xero 3-6mo as evidenced by an AUC of 0.78 (95%CI: 0.66–0.85; p < 0.0001), on plotting an ROC. (Fig. 4) Contra parotid glands post-RT SUV-median and mean planned RT dose stood out as the most statistically significant variables (p = 0.03 for both) followed by age at diagnosis (p = 0.06). Notably, mean ipsi parotid gland dose was detrimental to the predictive performance of this model as evidence by a 4-point decline in Bayesian Information Criteria (BIC) upon its omission. (Supplementary Table S3).

Discussion

In this study, we show that the median SUV of both, ipsilateral and contralateral parotid glands, decrease significantly after radiotherapy compared to baseline values. This was valid for nearly all dose levels, showing that even after very small radiation doses a change in SUV can
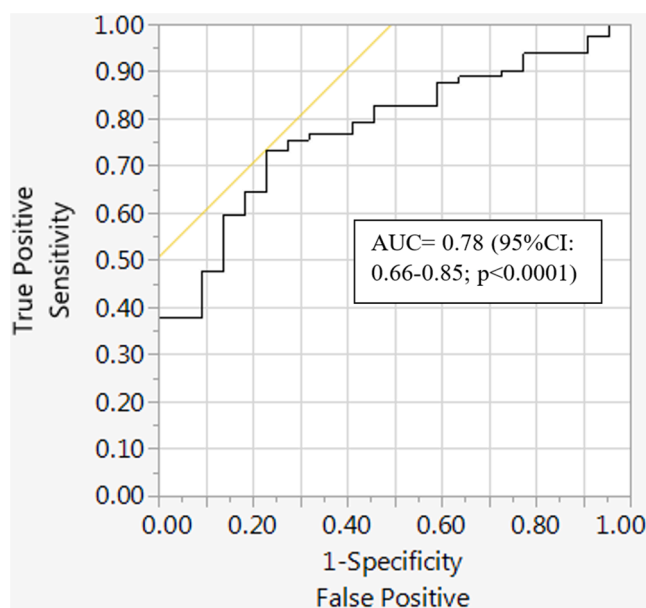
Fig. 4. Receiver Operator Characteristic Curve (ROC) displaying the model performance represented by area under the curve (AUC).

still be detected. One possible explanation of the decrease in median SUV is the reduction in acinar cells [16–19] with simultaneous increase of intercellular water or fat, which can be visualized in magnetic resonance imaging (MRI) by an increase in T2 [20,21] or ADC [22], and a rising fat fraction in DIXON MRI [20]. The direct negative correlation between ADC and FDG uptake [23] has been confirmed in several studies using a simultaneous PET/MR in pre-treatment HNC [24], lung cancer [25], lymphoma [26], and liver metastases [27] or post-RT as in rectal cancer [28] and retroperitoneal fibrosis [29].

Only five other studies have previously investigated the change in SUV of the parotid gland from pre- to post-radiotherapy (Table 2). Direct
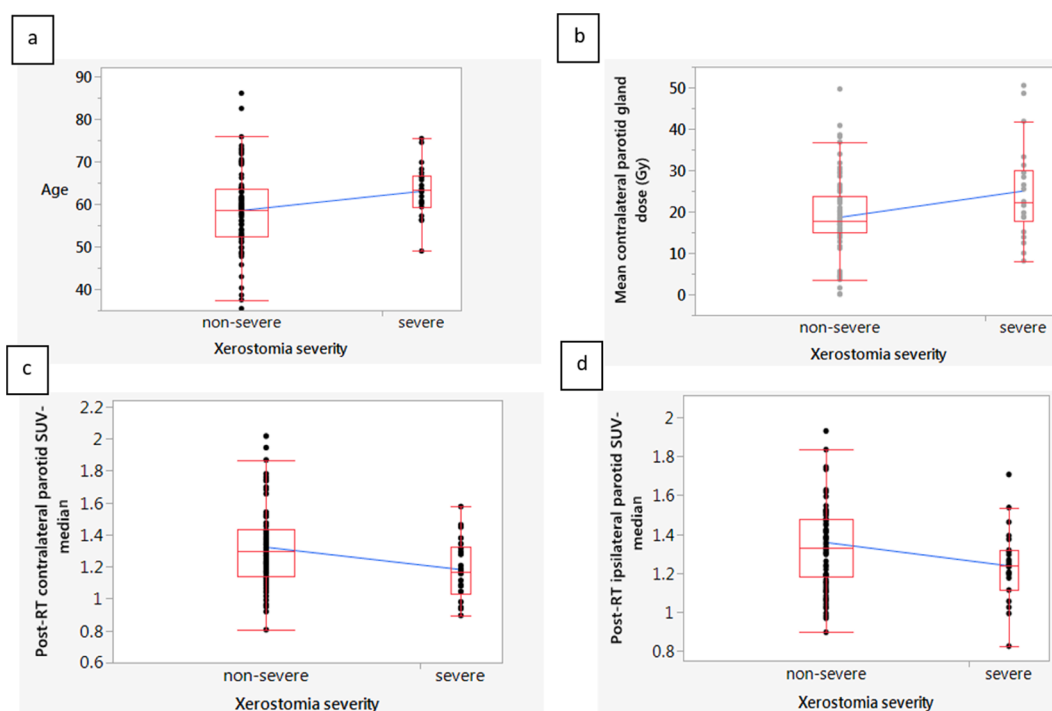
Fig. 3. Correlation between severity of post-radiotherapy xerostomia and (A) Age; (B) Mean contralateral parotid gland dose (Gy); (C) Post-radiotherapy contralateral parotid gland SUV-median; and (D) Post-radiotherapy ipsilateral parotid gland SUV-median.

Table 2

Overview of studies analyzing PET as biomarker of radiation-induced injury of the parotid glands. The comparison with our study is mainly hampered due to the missing correction for PET halo of FDG positive level II lymph nodes in most other studies (OP: oropharynx; L: larynx; HP: hypopharynx; NP: nasopharynx; OC: oral cavity; FDG: fluorodeoxyglucose; PET: positron emission tomography; RT: radiotherapy; IMRT: intensity modulated RT; VMAT: volumetric modulated arc therapy; w: weeks; m: months; BL: baseline; SUV: standardized uptake value; sign.:significantly; LNs: lymph nodes; HNC: head and neck cancers; NA: not applicable).

Author, year	N	Tumor entity	Node-positive disease	RT technique	PET tracer	Time point PET	Major findings Positive aspects/major limitations
Elhalawani,2019 (this study)	108	OP	99%	IMRT	18F-FDG	BL 3–6 m post-RT start (median 135 days)	Median SUV of ipsi- and contralateral parotid gland sign. decreased after RT; lower median SUV values post-RT (ipsi or post?), higher mean dose to the contralateral parotid gland and age sign. associated with severe xerostomia post-RT Pros: Patient number; OPC only; Correction for partial volume effects and SUV halo of level II LNs
Van Dijk 2018 [34]	161	HNC (OP, L, HP, NP, OC)	56%	IMRT (90%)/ VMAT (10%)	18F-FDG	BL	Xerostomia at BL, higher mean dose to the parotid gland and lower median and mean SUV of the parotid gland at BL were sign. associated with higher risk for xerostomia at 12 months (unclear if ipsi-, contralateral or both parotid glands) Pros: Patient number; prospective assessment of xerostomia at 12 m Cons: No full correction for partial volume effects and SUV halo of level II LNs; only BL PET imaging; dose received by the parotid glands unclear; no comparison between BL xerostomia and SUV
Cannon, 2012 [9]	98/ 14	HNC (OP, L, HP)	84%/93%	IMRT	18F-FDG	BL 7-9w post-RT	Mean fractional parotid SUV (=SUV post-tx/pre-tx; unclear if ipsi-, contralateral or both parotid glands) of 0.96 (range 0.62 – 1.85); stimulated saliva decreased post-RT to 41% relative to BL; neg. correlation between xerostomia grade and fractional SUV Pros: Subgroup of patients with prospectively assessed sialometry and xerostomia-specific questionnaire Cons: Unclear which SUV value has been used (i.e. median, mean, max); no correction for partial volume effects and SUV halo of level II LNs; xerostomia assessment in only 8 patients
Roach, 2012 [46]	49	HNC (OP, L, CUP, NP)	NA	IMRT	18F-FDG	BL 6-151w post-RT (mean 22w)	Mean SUVmean decreased by 5% with every 10 Gy increase in mean parotid gland dose; decrease in mean SUVmax by 8% with mean dose to the parotid gland of $\leq$ 20 Gy, and 46% with doses > 50 Gy Cons: No correction for partial volume effects and SUV halo of level II LNs; no xerostomia assessment; wide range of PET FU
Buus, 2006 [33]	12	HNC (L, OP, CUP, HP, OC)	50%	Ipsi wedged pair (3) OP (6), 3D (2), IMRT (1)	11C-methionine	8–54 m post-RT (median 21 m)	Net metabolic clearance of 11C-methionine neg. correlated with RT dose to the parotid gland; TD50 of 30 Gy (individual variation from 7 to 50 Gy) Pros: Correction for partial volume effects; correlation of net metabolic clearance of 11C-methionine and RT dose in parotid gland sub-volumes (5 Gy intervals) Cons: PET tracer not used in clinical routine; only 1 patient with IMRT and without hypoxic cell sensitizer; wide range of PET FU; low patient number
Buus, 2004 [47]	8	HNC (OP, CUP)	75%	Ipsi(5), IMRT (1), NA(2)	11C-methionine	BL (n = 2) 6–29 m post-RT (median 22 m; n = 6)	Higher 11C-radioactivity concentration in salivary glands (parotid and submandibular glands) receiving lower RT doses; net metabolic clearance of 11C-methionine neg. correlated with RT dose and pos. correlated to salivary gland function Pros: Saliva collection; dynamic PET scan Cons: PET tracer not used in clinical routine; no correction for partial volume effects and SUV halo of level II LN; only 1 patient with IMRT and without hypoxic cell sensitizer; different patients at baseline and post-RT; wide range of PET FU; low patient number
Rege, 1993 [48]	11	HNC (OP, Sinus, OC, NP, L)	40%	NA; Additional brachy-therapy (2)	18F-FDG	BL During RT 1-10w post-RT (usually 6w)	No sign. difference in FDG uptake between salivary glands "in field" or "out of field", and no sign. change with RT Pros: Analysis of parotid, submandibular and sublinguar glands; assessment also during RT; FDG uptake normalized on healthy cerebral tissue Cons: Parotid gland contour on only one slice pre-treatment, which has been copied and rotated to fit post-treatment scan; no correction for partial volume effects and SUV halo of level II LNs; dose received by the "in field" parotid glands unclear; 2 patients with additional brachytherapy; early post-RT PET scan; not the same patients for all time points; no correlation to xerostomia; low patient number

comparison between these studies and our results is challenging due to large differences in methodology and analysis. In our study, we only used the median SUV of the parotid glands for analysis. This was considered due to the fact that the SUV of the parotid gland can be largely affected by PET-positive lymph nodes in direct vicinity to the gland. Tumoral spread to these level II lymph nodes is specifically the case in locally advanced oral cavity, naso- and oropharyngeal cancers, which are among the most common head and neck tumors [30]. Not only the partial volume effect due to the voxel size matters, but also -and maybe more importantly- the halo around the FDG active tumor tissue, which can account for several millimeters, depending on the SUV window level [31,32]. This can have significant effect on the maximum SUV, and therefore also affects the mean SUV. To avoid at least the partial volume effect of surrounding tissue on the PET results, Buus et al. cropped their parotid gland structure by 5 mm. This was a sophisticated approach but resulted in some parotid gland volumes as low as 4 ml [33]. Unfortunately, subsequent PET image analysis of the parotid gland, published by other study groups, did not consider this confounding factor, although including lymph node positive oropharyngeal tumors in most cases (Table 2). Hence, the reported pre-treatment mean and maximum SUV values were most probably overestimated, whereas -due to tumor shrinkage- the post-treatment values would, if at all, only be slightly affected. Both will result in a falsely overestimated decrease in SUV mean and maximum after therapy, which will represent an effect of radio- and/or chemotherapy on the tumor rather than on the parotid gland.

Hence, a reasonable comparison of our study results could only be performed with the above-mentioned study of Buus et al. [33]. However, this study used ^{11}C-methionine as PET tracer and only one of their 12 patients received IMRT without a hypoxic cell sensitizer not to mention they reported the net clearance of the tracer rather than SUV values. The main finding of their study is the dose-dependency of the net clearance described as a sigmoid pattern. In our study however, although nearly 10 times more patients were studied, we couldn't see a dose dependency of the PET changes. One possible explanation could be the different median time interval between radiotherapy and PET scan which was 21 months in the study by Buus et al. and 3–6 months in our study. Probably, high doses to the parotid gland will result in prolonged damage, whereas low dose areas have the potential to still recover or recover faster from the RT-induced damage over time. To validate this, a longitudinal PET study needs to be conducted or more data from other studies need to be available. From MRI studies, we know that recovery of the parotid glands, measured as percent changes in volume or ADC values, most probably occurs after 6–8 months from end of RT [22].

On stratifying patients according to severity of xerostomia at 3–6 months post-RT, we found significantly lower median SUV values post-RT in the ipsi and contra parotid glands, higher mean contralateral parotid gland doses and a more elderly population in the patient subgroup that suffered from more severe symptoms. Of note, neither the pre-treatment median SUV, nor the percentage change in median SUV significantly correlated with xerostomia at 3–6 months, indicating that the post-treatment SUV is the most reliable PET image biomarker for assessment of xerostomia at that time point. Of note, none of the pre-RT SUV metrics were significantly associated with baseline xerostomia. However, van Dijk et al. could show a negative correlation of the baseline SUV values with xerostomia at twelve months post-RT [34]. Noteworthy, they have not analyzed the correlation between baseline SUV values and baseline xerostomia, and did not perform a second measurement during or post-RT.

Moreover, in our study a model combining post-RT median SUV of contralateral parotid gland with age and mean dose to contralateral parotid gland could correlate with the severity of post-RT xerostomia with demonstrable accuracy (AUC = 0.78). This shows that PET-derived imaging biomarkers can potentially play a role in evaluation of RT-induced normal tissue injury as previously demonstrated by our group using longitudinal CT and MRI studies [35–40].

Despite the strength of our study with the largest patient cohort having two PET assessments, before and after RT, inclusion of OPC patients only, compensation for partial volume effect and PET halo in the analysis and simultaneous physician-reported toxicity assessment - using a standardized tool (CTCAE v5.0) - with PET scan acquisition, our study has some limitations. First of all, our patients' cohort demonstrated a predominantly p16 positive subpopulation (91.6%), in a similar pattern to the US general population. [1]. Previous radiological studies described p16 positive OPC disease to often show larger cystic nodal metastases which might imply higher delivered radiation doses to nearby organs at risk, including parotid glands, when compared to their p16 negative counterparts. Nonetheless, the fact that our patients demonstrated a myriad p16 and nodal involvement combinations (Table 1), enabled us to study a wider spectrum of doses to parotid glands and corresponding changes in SUV.

Second, we noticed that parotid glands lateral edges shrank more compared to the medial portions, along the same lines as Robar et al observations [41]. Not surprisingly, the lateral edges are where the auto-contouring and deformable registration algorithms did not perform very well, requiring manual edits to the contours. These pitfalls could have added uncertainty to subsequent SUV and dose calculations. Hence, we decided not to include parotid gland volumetric changes in our analysis, since they are already well-documented in literature, and especially that the primary scope or our study is to assess longitudinal SUV changes as a surrogate for radiation-associated metabolic changes inside parotid glands. However, with our approach described above, to analyze the median SUV only, this might have had affected the PET results only to a minor extent and only in the dose level sub-volume analysis, when small regions at the edges were analyzed. Third, we only analyzed SUV changes in dose level sub-volumes up to 50 Gy to exclude possible PET halo effects of nearby FDG positive lymph nodes. We have chosen 50 Gy as nodal target volumes -including electively irradiated nodes- received at least 54 Gy and we assumed that the GTV to CTV/PTV margin and the dose falloff until 50 Gy will prevent the inclusion of any PET halo. Nevertheless, future analysis needs to be done to exactly assess the extent of such a PET halo and to find solutions for future analysis.

Another limitation is the fact, that although all PET scans have been performed within three to six months from the start of radiotherapy, they were not conducted at a standardized time point, potentially capturing parotid glands metabolic activity at varying recovery phases. However, contradicting results are available in the literature describing a decrease [42], increase [43] or stable values [44] for dry mouth between 2 and 6 months post-RT using the European Organization for Research and Treatment of Cancer (EORTC) H&N35 questionnaire. This could be also attributed in part to the highly subjective nature of xerostomia assessment -whether patient or physician reported- or the varying degrees of parotid glands recovery from subacute to chronic radiation-induced inflammation. Other pitfalls that our study shares with similar corollary studies to radiation symptom burden. Last, with the measurement after end of therapy, the ability to adapt the treatment according to changes in the FDG uptake is not possible anymore. Nevertheless, in our study we took the diagnostic post-treatment images for analysis to avoid further radiation to the patient with an additional mid-treatment scan. However, in MRI, changes in the parotid gland can be detected already during radiotherapy and predict for late xerostomia [45,46], so a prospective study with an additional mid-treatment PET scan seems to be justifiable.

In conclusion, temporal dynamics of PET-derived metrics manifest changes that can potentially serve as MIBs of RT-related parotid injury. Our results help generate hypothesis for the utility of integrating mid-RT PET-CT into adaptive RT trials for HNCs.

Declaration of Competing Interest

The authors declare that they have no known competing financial interests or personal relationships that could have appeared to influence

the work reported in this paper.

Acknowledgments

Appendix A. Supplementary data

Supplementary data to this article can be found online at https://doi.org/10.1016/j.ctro.2021.05.011.

References

[1] Gillison ML, Trotti AM, Harris J, Eisbruch A, Harari PM, Adelstein DJ, et al. Radiotherapy plus cetuximab or cisplatin in human papillomavirus-positive oropharyngeal cancer (NRG Oncology RTOG 1016): a randomised, multicentre, non-inferiority trial. Lancet 2019;393(10166):40–50.

[2] Vainshtein JM, Samuels S, Tao Y, Lyden T, Haxer M, Spector M, et al. Impact of xerostomia on dysphagia after chemotherapy-intensity-modulated radiotherapy for oropharyngeal cancer: Prospective longitudinal study. Head Neck 2016;38(S1):E1605–12.

[3] Sapir E, Tao Y, Feng F, Samuels S, El Naqa I, Murdoch-Kinch CA, et al. Predictors of Dysgeusia in Patients With Oropharyngeal Cancer Treated With Chemotherapy and Intensity Modulated Radiation Therapy. Int J Radiat Oncol Biol Phys 2016;96(2):354–61.

[4] Gupta N, Pal M, Rawat S, Grewal MS, Garg H, Chauhan D, et al. Radiation-induced dental caries, prevention and treatment - A systematic review. Natl J Maxillofac Surg 2015;6(2):160. https://doi.org/10.4103/0975-5950.183870.

[5] Janssens GO, Langendijk JA, Terhaard CH, Doornaert PA, van den Ende P, de Jong MA, et al. Quality-of-life after radiotherapy for advanced laryngeal cancer: Results of a phase III trial of the Dutch Head and Neck Society. Radiother Oncol 2016;119(2):213–20.

[6] Cliffe H, Patel C, Prestwich R, Scarsbrook A. Radiotherapy response evaluation using FDG PET-CT-established and emerging applications. Br J Radiol 2017;90 (1071):20160764. https://doi.org/10.1259/bjr.20160764.

[7] Mohamed ASR, Cardenas CE, Garden AS, Awan MJ, Rock CD, Westergaard SA, et al. Patterns-of-failure guided biological target volume definition for head and neck cancer patients: FDG-PET and dosimetric analysis of dose escalation candidate subregions. Radiother Oncol 2017;124(2):248–55.

[8] Elhalawani H, Volpe S, Cardenas CE, Barua S, Rock C, Lin T, et al. Development of Temporal Dose-Weighted Positron Emission Tomography Metabolic Imaging Biomarkers (PET MIBs) of Radiation-Related Parotid Glands Injury in Oropharyngeal Cancer Patients. Int J Radiat Oncol Biol Phys 2018;102(3):e240–1.

[9] Cannon B, Schwartz DL, Dong L. Metabolic imaging biomarkers of postradiotherapy xerostomia. Int J Radiat Oncol Biol Phys 2012;83(5):1609–16.

[10] Stieb S, Kiser K, van Dijk L, Livingstone NR, Elhalawani H, Elgohari B, et al. Imaging for Response Assessment in Radiation Oncology: Current and Emerging Techniques. Hematol Oncol Clin North Am 2020;34(1):293–306.

[11] Freymann JB, Kirby JS, Perry JH, Clunie DA, Jaffe CC. Image Data Sharing for Biomedical Research—Meeting HIPAA Requirements for De-identification. J Digit Imaging 2012;25(1):14–24.

[12] Lin TA, Garden AS, Elhalawani H, Elgohari B, Jethanandani A, Ng SP, et al. Radiographic retropharyngeal lymph node involvement in HPV-associated oropharyngeal carcinoma: Patterns of involvement and impact on patient outcomes. Cancer 2019;125(9):1536–46.

[13] Cardenas CE, Mohamed ASR, Tao R, Wong AJR, Awan MJ, Kuruvila S, et al. Prospective Qualitative and Quantitative Analysis of Real-Time Peer Review Quality Assurance Rounds Incorporating Direct Physical Examination for Head and Neck Cancer Radiation Therapy. Int J Radiat Oncol Biol Phys 2017;98(3):532–40.

[14] https://ctep.cancer.gov/protocoldevelopment/electronic_applications/doc s/CTCAE_v5_Quick_Reference_8.5x11.pdf [Accessed on April 09, 2019].

[15] Moeller BJ, Rana V, Cannon BA, Williams MD, Sturgis EM, Ginsberg LE, et al. Prospective risk-adjusted [18F]Fluorodeoxyglucose positron emission tomography and computed tomography assessment of radiation response in head and neck cancer. J Clin Oncol 2009;27(15):2509–15.

[16] Teshima K, Murakami R, Yoshida R, Nakayama H, Hiraki A, Hirai T, et al. Histopathological changes in parotid and submandibular glands of patients treated with preoperative chemoradiation therapy for oral cancer. J Radiat Res 2012;53 (3):492–6.

[17] Stramandinoli-Zanicotti RT, Sassi LM, Schussel JL, Torres MF, Funchal M, Smaniotto GH, et al. Effect of fractionated radiotherapy on the parotid gland: an experimental study in Brazilian minipigs. Int Arch Otorhinolaryngol 2013;17(2):163–7.

[18] Radfar L, Sirois DA. Structural and functional injury in minipig salivary glands following fractionated exposure to 70 Gy of ionizing radiation: an animal model for human radiation-induced salivary gland injury. Oral Surg Oral Med Oral Pathol Oral Radiol Endod. 2003;96(3):267–74.

[19] Price RE, Ang KK, Stephens LC, Peters LJ. Effects of continuous hyperfractionated accelerated and conventionally fractionated radiotherapy on the parotid and submandibular salivary glands of rhesus monkeys. Radiother Oncol 1995;34(1):39–46.

[20] Zhou N, Chu C, Dou X, Chen W, He J, Yan J, et al. Early evaluation of radiation-induced parotid damage in patients with nasopharyngeal carcinoma by T2 mapping and mDIXON Quant imaging: initial findings. Radiat Oncol 2018;13(1). https://doi.org/10.1186/s13014-018-0970-9.

[21] Houweling AC, Schakel T, van den Berg CAT, Philippens MEP, Roesink JM, Terhaard CHJ, et al. MRI to quantify early radiation-induced changes in the salivary glands. Radiother Oncol 2011;100(3):386–9.

[22] Stieb S, Elgohari B, Fuller CD. Repetitive MRI of organs at risk in head and neck cancer patients undergoing radiotherapy. Clin Trans Radiat Oncol 2019;18:131–9.

[23] Deng S, Wu Z, Wu Y, Zhang W, Li J, Dai Na, et al. Meta-Analysis of the Correlation between Apparent Diffusion Coefficient and Standardized Uptake Value in Malignant Disease. Contrast Media Mol Imaging 2017;2017:1–16.

[24] Zwirner K, Thorwarth D, Winter RM, Welz S, Weiss J, Schwenzer NF, et al. Voxel-wise correlation of functional imaging parameters in HNSCC patients receiving PET/MRI in an irradiation setupVoxelweise Korrelation funktioneller PET/MRT-Parameter in Bestrahlungslagerung bei Patienten mit Kopf-Hals-Tumoren. Strahlenther Onkol 2018;194(8):719–26.

[25] Usuda K, Funasaki A, Sekimura A, Motono N, Matoba M, Doai M, et al. FDG-PET/ CT and diffusion-weighted imaging for resected lung cancer: correlation of maximum standardized uptake value and apparent diffusion coefficient value with prognostic factors. Med Oncol 2018;35(5). https://doi.org/10.1007/s12032-018-1128-1.

[26] Bernstine H, Domachevsky L, Nidam M, Goldberg N, Abadi-Korek I, Shpilberg O, et al. 18F-FDG PET/MR imaging of lymphoma nodal target lesions: Comparison of PET standardized uptake value (SUV) with MR apparent diffusion coefficient (ADC). Medicine (Baltimore) 2018;97(16). e0490-e.

[27] Stein D, Goldberg N, Domachevsky L, Bernstine H, Nidam M, Abadi-Korek I, et al. Quantitative biomarkers for liver metastases: comparison of MRI diffusion-weighted imaging heterogeneity index and fluorine-18-fluoro-deoxyglucose standardised uptake value in hybrid PET/MR. Clin Radiol 2018;73(9). 832.e17-e22.

[28] Cerny M, Dunet V, Rebecchini C, Hahnloser D, Prior J, Sempoux C, et al. Response of locally advanced rectal cancer (LARC) to radiochemotherapy: DW-MRI and multiparametric PET/CT in correlation with histopathology. Nuklearmedizin 2019; 58(01):28–38.

[29] Ruhlmann V, Poeppel TD, Brandt AS, Grüneisen J, Ruhlmann M, Theysohn JM, et al. (18)F-FDG PET/MRI evaluation of retroperitoneal fibrosis: a simultaneous multiparametric approach for diagnosing active disease. Eur J Nucl Med Mol Imaging 2016;43(9):1646–52.

[30] Shield KD, Ferlay J, Jemal A, Sankaranarayanan R, Chaturvedi AK, Bray F, et al. The global incidence of lip, oral cavity, and pharyngeal cancers by subsite in 2012. CA Cancer J Clin 2017;67(1):51–64.

[31] Yip SSF, Aerts HJWL. Applications and limitations of radiomics. Phys Med Biol 2016;61(13):R150–66.

[32] Milgrom SA, Elhalawani H, Lee J, Wang Q, Mohamed ASR, Dabaja BS, et al. A PET Radiomics Model to Predict Refractory Mediastinal Hodgkin Lymphoma. Sci Rep 2019;9(1). https://doi.org/10.1038/s41598-018-37197-z.

[33] Buus S, Grau C, Munk OL, Rodell A, Jensen K, Mouridsen K, et al. Individual radiation response of parotid glands investigated by dynamic 11C-methionine PET. Radiother Oncol 2006;78(3):262–9.

[34] van Dijk LV, Noordzij W, Brouwer CL, Boellaard R, Burgerhof JGM, Langendijk JA, et al. (18)F-FDG PET image biomarkers improve prediction of late radiation-induced xerostomia. Radiother Oncol 2018;126(1):89–95.

[35] Elhalawani H, Jin Y, Li T, Randall JW, Mahajan A, Mohamed AS, et al. Longitudinal and Dose Dependent Analysis on White Matter Injury in Glioblastoma Radiation Therapy. Int J Radiat Oncol Biol Phys 2019;105(1):S231. https://doi.org/10.1016/j.ijrobp.2019.06.330.

[36] Mohamed ASR, He R, Ding Y, Wang J, Fahim J, Elgohari B, et al. Prospective assessment of DCE-MRI parameters associated with advanced mandibular osteoradionecrosis after IMRT for head and neck cancer. medRxiv. 2019: 2019.12.23.19015651.

[37] Meheissen MAM, Mohamed ASR, Kamal M, Hernandez M, Volpe S, Elhalawani H, et al. A prospective longitudinal assessment of MRI signal intensity kinetics of non-target muscles in patients with advanced stage oropharyngeal cancer in relationship to radiotherapy dose and post-treatment radiation-associated dysphagia: Preliminary findings from a randomized trial. Radiother Oncol 2019; 130:46–55.

[38] Elgohari B, Mohamed AS, Ng SP, Elhalawani H, Elsayes AK, He R, et al. Diffusion-Weighted MRI As an Early Biomarker of Xerostomia in Oropharyngeal Cancer Patients Treated with Radiation Therapy. Int J Radiat Oncol Biol Phys 2018;102 (3):e214–5.

[39] Elhalawani H, Mohamed ASR, Kanwar A, Dursteler A, Rock CD, Eraj SE, et al. EP-2121: Serial Parotid Gland Radiomic-based Model Predicts Post-Radiation Xerostomia in Oropharyngeal Cancer. Radiother Oncol 2018;127:S1167–8.

[40] Elhalawani H, Volpe S, Barua S, Mohamed A, Yang P, Ng SP, et al. Exploration of an Early Imaging Biomarker of Osteoradionecrosis in Oropharyngeal Cancer Patients: Case-Control Study of the Temporal Changes of Mandibular Radiomics Features. Int J Radiat Oncol Biol Phys 2018;100(5):1363–4.

[41] Robar JL, Day A, Clancey J, Kelly R, Yewondwossen M, Hollenhorst H, et al. Spatial and dosimetric variability of organs at risk in head-and-neck intensity-modulated radiotherapy. Int J Radiat Oncol Biol Phys 2007;68(4):1121–30.

[42] Rathod S, Gupta T, Ghosh-Laskar S, Murthy V, Budrukkar A, Agarwal JP. Quality-of-life (QOL) outcomes in patients with head and neck squamous cell carcinoma (HNSCC) treated with intensity-modulated radiation therapy (IMRT) compared to

three-dimensional conformal radiotherapy (3D-CRT): Evidence from a prospective randomized study. Oral Oncol 2013;49(6):634–42.

[43] Pow EHN, Kwong DLW, McMillan AS, Wong MCM, Sham JST, Leung LHT, et al. Xerostomia and quality of life after intensity-modulated radiotherapy vs. conventional radiotherapy for early-stage nasopharyngeal carcinoma: Initial report on a randomized controlled clinical trial. Int J Radiat Oncol Biol Phys 2006;66(4): 981–91.

[44] Tribius S, Raguse M, Voigt C, Münscher A, Gröbe A, Petersen C, et al. Residual deficits in quality of life one year after intensity-modulated radiotherapy for patients with locally advanced head and neck cancer: Results of a prospective studyResiduale Defizite in der Lebensqualität ein Jahr nach intensitätsmodulierter Strahlentherapie bei Patienten mit lokal fortgeschrittenen Kopf-Hals-Tumoren: Ergebnisse einer prospektiven Studie. Strahlenther Onkol 2015;191(6):501–10.

[45] Zhang Q, Wei Y-M, Qi Y-G, Li B-S. Early Changes in Apparent Diffusion Coefficient for Salivary Glands during Radiotherapy for Nasopharyngeal Carcinoma Associated with Xerostomia. Korean J Radiol 2018;19(2):328–33.

[46] Juan C-J, Cheng C-C, Chiu S-C, Jen Y-M, Liu Y-J, Chiu H-C, et al. Temporal evolution of parotid volume and parotid apparent diffusion coefficient in nasopharyngeal carcinoma patients treated by intensity-modulated radiotherapy investigated by magnetic resonance imaging: a pilot study. PLoS One 2015;10(8). e0137073-e.

[47] Buus S, Grau C, Munk OL, Bender D, Jensen K, Keiding S. 11C-methionine PET, a novel method for measuring regional salivary gland function after radiotherapy of head and neck cancer. Radiother Oncol 2004;73(3):289–96.

[48] Rege SD, Chaiken L, Hoh CK, Choi Y, Lufkin R, Anzai Y, et al. Change induced by radiation therapy in FDG uptake in normal and malignant structures of the head and neck: quantitation with PET. Radiology 1993;189(3):807–12.